

# Impact of Deep Water Formation on Antarctic Circumpolar Transport During Gateway Opening

D. R. Munday<sup>1</sup> , I. Sauermilch<sup>2</sup> , A. Klocker<sup>3</sup> , J. M. Whittaker<sup>4</sup> 

<sup>1</sup>British Antarctic Survey, Cambridge, UK

<sup>2</sup>Department of Earth Sciences, University of Utrecht, Utrecht, Netherlands

<sup>3</sup>NORCE Norwegian Research Centre, Bjerknes Centre for Climate Research, Bergen, Norway

<sup>4</sup>Institute for Marine and Antarctic Studies, University of Tasmania, Hobart, Australia.

## Key Points:

- Deep water formation in the Southern Ocean enhances Antarctic Circumpolar Current transport.
- Circumpolar transport is possible even with large obstacles to the flow.
- Deep water formation enables transport north of Australia with a narrow Tasman Gateway.

---

Corresponding author: David R. Munday, [danday@bas.ac.uk](mailto:danday@bas.ac.uk)

## Abstract

Ambiguity over the Eocene opening times of the Tasman Gateway and Drake Passage makes it difficult to determine the initiation time of the Antarctic Circumpolar Current (ACC). If the Tasman Gateway opened later than Drake Passage, then Australia may have prevented the proto-ACC from forming. Recent modelling results have shown that only a relatively weak circumpolar transport results under Eocene surface forcing. This leads to warm and buoyant coastal water around Antarctica, which may impede the formation of deep waters and convective processes. This suggests that a change in deep water formation might be required to increase the density contrast across the Southern Ocean and increase circumpolar transport.

Here we use a simple reduced gravity model with two basins, to represent the Atlantic and the Pacific. This fixes the density difference between surface and deep water and allows us to isolate the impact of deep water formation on circumpolar transport. With no obstacle on the southern boundary the circumpolar current increases its transport from 82.3 to 270.0 Sv with deep water formation. Placing an Antipodean landmass on the southern boundary reduces this transport as the landmass increases in size. However, circumpolar flow north of this landmass remains a possibility even without deep water formation. Weak circumpolar transport continues until the basin is completely blocked by the Antipodes. When the Antipodes is instead allowed to split from the southern boundary, circumpolar transport recovers to its unobstructed value. Flow rapidly switches to south of the Antipodes when the gateway is narrow.

## 1 Introduction

In the modern world, the Southern Ocean is the only body of water to completely circumnavigate the globe. In doing so it connects the other ocean basins via its major current systems, the Antarctic Circumpolar Current (ACC, in the horizontal plane) and the Residual Meridional Overturning Circulation (RMOC, in the vertical-meridional plane). The volume transport of the ACC, at around  $137 \pm 7$  Sv [Sverdrup,  $1 \text{ Sv} = 10^6 \text{ m}^3 \text{ s}^{-1}$  Meredith *et al.*, 2011] [ $173 \pm 10.17$  Sv including the near bottom flow measured by current meters, Donohue *et al.*, 2016], is the largest observed for any modern current system. However, over geological time there has been major tectonic reorganisation of Southern Ocean gateways, i.e. the Tasman Gateway and Drake Passage. Changes to these gateways, in terms of their width and depth, could have a major influence on the strength of the ACC, or even preclude its existence [e.g. Kennett, 1977; Hill *et al.*, 2013; Baatsen *et al.*, 2018].

Unfortunately, there is considerable ambiguity to the opening time and evolution of both Southern Ocean gateways. For example, the opening of Drake Passage may span from 50Ma to 17Ma [Livermore *et al.*, 2005; Barker *et al.*, 2007], with a similar range for the inception of the ACC [Wei and Wise, 1992; Scher and Martin, 2006]. Other measurements suggest that Drake Passage may have been open during the Cretaceous and subsequently closed prior to a later reopening [van de Lagemaat *et al.*, 2021]. Similarly, the earliest dates for a shallow opening of the Tasman Gateway are also 50Ma [Bijl *et al.*, 2013] with a deep seaway between the Indian and Pacific basins in place by 35-32Ma [Royer and Rollet, 1997] and the potential for a relatively rapid subsidence history [Stickley *et al.*, 2004]. Dredged sediment samples further suggest that rapid ACC flow through the Tasman Gateway might not have occurred for another 3-5 million years, when the gateway was aligned with the westerly wind jet [Scher *et al.*, 2015]. On the north side of Australia, the Indonesian throughflow was likely open during the Eocene, narrowing after 30Ma [Gaina and Müller, 2007]. This may have worked as a “northern gateway” for a young ACC assuming an open Drake Passage  $> 30$  Ma [Sijp *et al.*, 2011]. This evidence suggests that the inception and early evolution of the ACC’s transport was likely affected by a series of tectonic changes, over millions of years, to the sea-floor bathymetry and ocean

65 gateways.

66 There are strong theoretical grounds to expect the position of the ACC to be tied to  
 67 major bathymetric obstacles [Marshall, 1995]. However, simple models and theory also  
 68 show it has the ability to migrate to follow wind forcing to a quite astonishing degree [Al-  
 69 lison *et al.*, 2010; Marshall *et al.*, 2016]. This led Munday *et al.* [2015] to suggest that the  
 70 opening of the Tasman Gateway might not be a prerequisite for a circumpolar current,  
 71 as has sometimes been assumed in the literature [see, e.g., Barker *et al.*, 2007; Sijp *et al.*,  
 72 2014]. The idealised channel model of Munday *et al.* [2015] indicates that overlapping  
 73 continental barriers do not prevent circumpolar transport in the range of several 10's of  
 74 Sv, as long as there is a traceable circumpolar path around the continents. Using plausi-  
 75 ble bathymetric reconstructions, and forcing derived from the coupled climate model of  
 76 Hutchinson *et al.* [2018], Sauermilch *et al.* [2021] show that both gateways must be open  
 77 and deeper than 300m to allow significant circumpolar flow. In their supplementary case  
 78 with Australia attached to Antarctica, no circumpolar flow results. They hypothesise that  
 79 initiation and/or strengthening of deep water formation and the continuously decreas-  
 80 ing atmospheric carbon dioxide concentrations around Antarctica may play a role in the  
 81 strengthening of the ACC to present-day conditions and in setting its transport.

82 Global climate change during the Late Eocene, and across the Eocene-Oligocene  
 83 transition (34 Ma), is accompanied by progressive global cooling, including that of the  
 84 deep water [see, e.g. Westerhold *et al.*, 2020]. This is interlinked with the reorganisation of  
 85 ocean circulation, as well as changes in the sources and strength of deep water formation.  
 86 Uncertainties remain about the rate and location of deep-water formation during and prior  
 87 to the Eocene. However, modelling and geochemical studies (primarily isotopic composi-  
 88 tion analyses on sediment cores) agree on a bipolar deep water formation; deep water is  
 89 formed in the North and South Pacific, as well as in the Southern Ocean's Atlantic sector  
 90 [see, e.g. Hague *et al.*, 2012; Thomas, 2004; Thomas *et al.*, 2014; Via and Thomas, 2006;  
 91 McKinley *et al.*, 2019].

92 Some evidence exists that during and prior to the Eocene, meridional overturning  
 93 circulation was active in the Pacific Ocean (albeit weaker than in the modern-day). This  
 94 gradually switched to the Atlantic around 36 Ma and onwards [McKinley *et al.*, 2019]. Lo-  
 95 cally focused bottom water formation took place offshore of Antarctica [Huck *et al.*, 2017]  
 96 and, with the onset of Antarctic-wide glaciation around 34 Ma, sea ice became present  
 97 and Antarctic coastal waters cooled down. Together with the increased Antarctic-ward  
 98 salt flux within the Ekman layer, the dense and cool water masses subsided to the abyssal  
 99 plain regions offshore the Antarctic shorelines [Goldner *et al.*, 2014]. This deep water for-  
 100 mation enhanced the meridional overturning circulation and contributed to the global deep  
 101 water cooling observed by oxygen isotope records [see, e.g. Westerhold *et al.*, 2020].

102 The development of the proto-ACC caused North Atlantic deep water formation  
 103 onset, affecting the meridional overturning circulation, as well as leading to deep-ocean  
 104 circulation, and the onset of modern-like bipolar deep water formation [see, e.g. Via and  
 105 Thomas, 2006]. Oxygen isotope records suggest that from the early Oligocene onwards,  
 106 ocean waters started to develop modern-day-like surface, intermediate, deep and bottom  
 107 water layers, caused by the strengthening of the proto-ACC [Katz *et al.*, 2011]. The ACC  
 108 initiation also lead to thermal differentiation between North Atlantic and Southern Ocean  
 109 deep waters [Borrelli *et al.*, 2014]. This suggests that there is indeed a strong link between  
 110 ACC transport and deep water formation, as hypothesised by Sauermilch *et al.* [2021].

111 The questions we seek to answer here are

- 112 1. Does the initiation of deep water formation around Antarctica influence the circum-  
 113 polar transport of the ACC?
- 114 2. Can the presence of deep water formation lead to circumpolar transport when the  
 115 Tasman Gateway is closed?

116 Given the uncertainty regarding continental geometry and surface forcing, we choose  
 117 to investigate the above questions using an idealised numerical model in a process study  
 118 framework. Our aim is not to simulate a circumpolar current in a realistically complex  
 119 geometry, but to investigate the relevance of theoretical ideas based on the modern ACC  
 120 to its inception and early history. By using a reduced gravity model with restoring to a  
 121 shallow layer thickness near the southern continental boundary, we can choose the pres-  
 122 ence or absence of deep water formation. This would not be possible in a more complex  
 123 3D model, since the combination of different forcing patterns would determine the pres-  
 124 ence/absence of deep water formation as an emergent property of the model solution. A  
 125 reduced gravity model also has the benefit of allowing us to draw on a substantial body  
 126 of literature regarding the spin-up and adjustment of the ACC [see, e.g., *Allison, 2009*;  
 127 *Allison et al., 2010, 2011*], making for a well-understood framework to hang our problem  
 128 on.

129 In Section 2 we describe the details of our reduced gravity model and the diagnostic  
 130 methods we apply to it. In Section 3, we discuss the results of the reduced gravity model  
 131 experiments aimed at answering the above questions. We split these experiments into two  
 132 sets. The first set, regarding the migration of the ACC around a landmass on the southern  
 133 boundary as it increases in northwards extent (Sections 3.2), and the second set regarding  
 134 a landmass separating from the southern boundary and migrating northwards (3.3). We  
 135 close with a summary of our conclusions and discussion of our results in Section 4.

## 136 2 Methods

### 137 2.1 Model Numerics and Domain

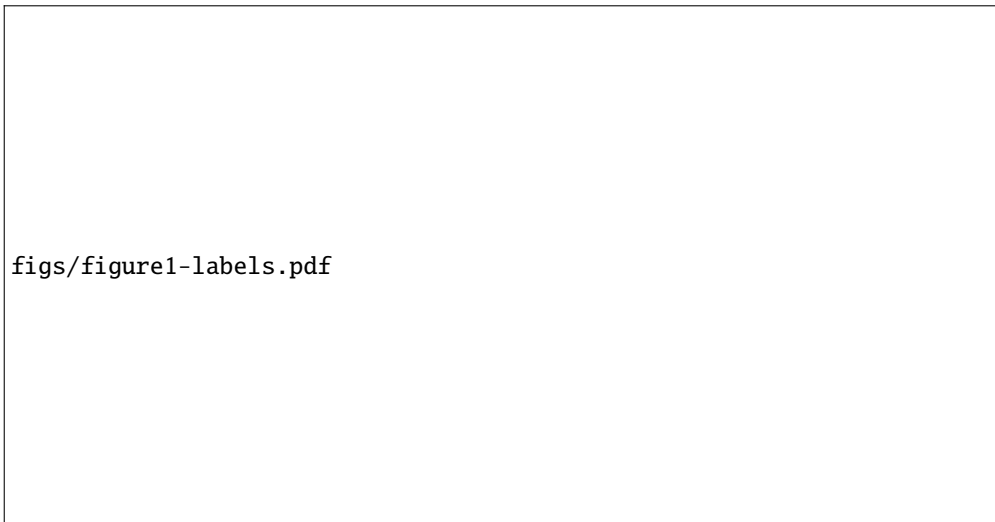
138 For our idealised numerical experiments, we choose to use a reduced gravity formu-  
 139 lation comprised of a single active layer overlying a motionless abyss of slightly denser  
 140 water. This abyss is assumed to be of infinite depth, such that its velocity can be consid-  
 141 ered to be zero, and to completely encompass any bathymetry. The equations of motion  
 142 for this model are written in vector-invariant form and given by

$$143 \frac{\partial \mathbf{u}}{\partial t} + (f + \xi) \mathbf{k} \times \mathbf{u} = -\nabla B + \frac{1}{h} \nabla \cdot (A_H h \nabla \mathbf{u}) + \frac{\boldsymbol{\tau}}{\rho_0 h}, \quad (1)$$

$$144 \frac{\partial h}{\partial t} + \nabla \cdot (h \mathbf{u}) = \nabla \cdot (\kappa_{GM} \nabla h) + \frac{\kappa_v}{h} - \gamma (h - h^*), \quad (2)$$

149 where  $\mathbf{u} = (u, v)$  and  $h$  are the two-dimensional flow velocity and thickness of the ac-  
 150 tive fluid layer, respectively. The Bernoulli potential is given by  $B = g'h + \frac{1}{2} \mathbf{u} \cdot \mathbf{u}$ , with  
 151  $g' = g\Delta\rho/\rho_0$  being the reduced gravity. The Boussinesq reference density of the active  
 152 layer is  $\rho_0$  and the density difference between the active layer and the motionless abyss  
 153 is  $\Delta\rho$ . The grid spacing is  $1^\circ$  in both longitude and latitude, so the zonal grid spacing in  
 154 kilometres decreases towards the northern/southern high latitudes. The standard values  
 155 used for the model parameters, along with details of the timestep, etc, are given in Table  
 156 1. Note that for reasons of numerical stability we found it necessary to half the timestep  
 157 for experiments without deep water formation.

158 Each numerical experiment is run for sufficiently long to reach its final equilibrium.  
 159 We define equilibrium as being attained when the absolute and relative change between  
 160 circumpolar transport values 30 days apart are less than  $2 \times 10^{-5}$  Sv and  $1 \times 10^{-6}$ , respec-  
 161 tively. This can take anywhere from 2000 to 30 000 model years. A single experiment  
 162 without deep water formation does not meet these criteria. This experiment has its An-  
 163 tipodean land mass (see below) extending from the southern to the northern boundary and  
 164 has a total circumpolar transport of only  $-0.0553$  Sv; it is the only experiment to have a  
 165 net westward circumpolar transport. The absolute change in transport for this experiment  
 166 is only  $0.01 \times 10^{-5}$  Sv, which is the smallest of all the experiments, and so we deem that  
 167 this is sufficiently spun up for our purposes.



146 **Figure 1.** Schematic of the model domain and the applied wind stress. The solid northern/southern bound-  
 147 aries and the partial barriers described in the test are in black. The area shaded grey is the “Antipodes” and  
 148 the dotted line is the Equator. The line graph to the left is the applied zonal wind stress.

168 The momentum equation, Equation (1), incorporates viscosity with a constant grid  
 169 Reynolds number such that the viscosity,  $A_H$ , varies with latitude. This prevents the model  
 170 from violating stability constraints near the northern/southern boundary where the longitu-  
 171 dinal grid spacing is much smaller than the meridional grid spacing. Surface wind forcing  
 172 of strength  $\tau$  is applied as a body force over the active fluid layer. The Coriolis and vortex  
 173 force terms are calculated so as to conserve enstrophy and KE is calculated to also ensure  
 174 its conservation.

175 The continuity equation, Equation (2), incorporates the *Gent and McWilliams* [1990]  
 176 eddy parameterisation as thickness diffusivity, written as an advective flux with a constant  
 177 co-efficient of  $\kappa_{GM}$ . This acts as a zero-order eddy parameterisation in this model frame-  
 178 work and acts to reduce gradients in thickness in a similar manner to baroclinic instability,  
 179 as it tends to flatten isopycnals. These simulations therefore have more in common with  
 180 the  $1^\circ$  Supplementary cases of *Sauermilch et al.* [2021] than they do their  $1/4^\circ$  simula-  
 181 tions, i.e. they are viscous/diffusive and lack resolved mesoscale eddies. The model also  
 182 includes a parameterisation of diapycnal diffusivity as per *Gnanadesikan* [1999], with a  
 183 constant co-efficient of  $\kappa_V$ . When the active fluid layer is thin, this acts to flux volume up-  
 184 wards and thicken the layer, which is equivalent to heat being fluxed downwards. We ne-  
 185 glect any parameterisation of northern sinking, as included in the model of *Gnanadesikan*  
 186 [1999] or those of *Nof* [2000, 2002, 2003], as per *Allison* [2009] and *Allison et al.* [2010,  
 187 2011].

188 Within  $\sim 3^\circ$  of the southern boundary, the thickness of the active layer is strongly  
 189 restored to a small value, given by  $h^*$  (see Table 1). This restoring takes place with a  
 190 timescale of  $t_{\text{restore}}$  and is intended to mimic the effect of cooling close to Antarctica,  
 191 which leads to the thickness of the active layer becoming small in this region. For numer-  
 192 ical reasons, the value of  $h^*$  is also enforced as a minimum surface thickness throughout  
 193 the domain. This prevents numerical instability if the layer outcrops (goes to zero thick-  
 194 ness) and, roughly speaking, parameterises buoyancy forcing and/or mode water formation.  
 195 This term in Equation (2) represents deep water formation via buoyancy loss to the atmo-  
 196 sphere near Antarctica. By setting  $t_{\text{restore}} = \infty$  ( $\gamma = 0.0$ ), we are able to disable deep water  
 197 formation and test our hypotheses.

216

**Table 1.** Standard Parameter Values for Reduced Gravity Model

Parameter	Symbol	Value	Units
Diapycnal diffusivity	$\kappa_v$	$10^{-5}$	$\text{m}^2/\text{s}$
GM co-efficient	$\kappa_{GM}$	2000	$\text{m}^2/\text{s}$
Grid length scale (mean grid spacing)	$L$	-	$m$
Grid Reynolds number	$\text{Re}_\Delta$	0.0062	-
Grid spacing (long,lat)	$\Delta\lambda, \Delta\phi$	1, 1	$^\circ$
Horizontal viscosity	$A_H$	$\text{Re}_\Delta L^2/4\Delta t$	$\text{m}^2/\text{s}$
Peak wind stress	$\tau_0$	0.15	$\text{N}/\text{m}^2$
Reduced gravity	$g'$	0.02	$\text{m}/\text{s}^2$
Restoring thickness	$h^*$	10	$m$
Restoring timescale ( $1/\gamma$ )	$t_{\text{restore}}$	$10^6$	$s$
Timestep	$\Delta t$	600/1200	$s$

198 The model equations are stepped forwards in time using the Adams-Bashforth 3rd  
199 order scheme, due to its advantages over a centred-in-time scheme [Durrant, 1991]. The  
200 continuity equation is discretised using centred 2nd order differencing, which conserves  
201 volume. Apart from the timestepping method, the model formulation is roughly the same  
202 as that used in Allison *et al.* [2010] and Allison *et al.* [2011], although details of, e.g., wind  
203 stress forcing are altered to suit the problem at hand. The model uses spherical polar co-  
204 ordinates and velocity boundary conditions are applied using ghost points. Ghost points  
205 can lead to the underestimation of viscous stresses near boundaries [Adcroft and Marshall,  
206 1998]. However, our emphasis here is on traceability to previous work and simplicity.

207 The wind forcing is given by the following simple analytic expression

$$208 \tau_x = \begin{cases} 0 & \text{if } \phi > -39^\circ, \\ \tau_0 \cos^2(\pi(\phi + 54.5)/30) & \text{if } -69.5^\circ \leq \phi \leq -39.5^\circ, \\ 0 & \text{if } \phi < -70^\circ, \end{cases} \quad (3)$$

209  $\tau_y = 0,$

210

211 where  $\tau = (\tau_x, \tau_y)$ ,  $\tau_0$  is the peak wind stress and  $\phi$  is the latitude in degrees. This places  
212 the peak wind at  $54.5^\circ\text{S}$  and makes a cosine-bell  $30^\circ$  wide (allowing for grid staggering).  
213 This ensures that the wind stress is zero within the region of deep water formation (if  
214 present), to prevent any numerical issues, and to the north of the southern tip of “Africa”.  
215 The shape of this idealised wind profile is shown in the left-hand panel of Figure 1.

217 The idealised continental geometry is shown in Figure 1. It consists of two ocean  
218 basins connected by two partial barriers to the flow. The southern boundary is at  $74^\circ\text{S}$   
219 and the northern boundary is at  $65^\circ\text{N}$ . This configuration is similar to that used by Allison  
220 *et al.* [2010] and Allison *et al.* [2011], with the addition of a second ocean basin and an  
221 accompanying second barrier to the flow.

222 The left-hand basin in Figure 1 is  $120^\circ$  wide in longitude; we identify this basin  
223 with, and refer to it as, the Indo-Pacific basin. The right-hand basin is  $60^\circ$  wide in lon-  
224 gitude; we identify this basin with, and refer to it as, the Atlantic basin. The two partial  
225 barriers between the basins are both  $16^\circ$  wide. The barrier to the west of the Indo-Pacific  
226 basin begins at  $38^\circ\text{S}$  and extends northwards to the northern boundary. This barrier rep-  
227 represents the continental landmass made up by Europe, Africa, and Asia. The barrier to the  
228 west of the Atlantic basin begins at  $64^\circ\text{S}$  and extends northwards to the northern bound-  
229 ary. This barrier represents the landmass made up of North and South America and the  
230 narrower constriction between it and the southern boundary represents Drake Passage.

231 The grey-shaded region in Figure 1 is the “Antipodes”, a landmass added to the  
 232 southern boundary to act as our model’s analogue of Australia, Tasmania, and Zealandia.  
 233 This landmass is always 20° wide in longitude, which is the scaled width of the modern  
 234 Antipodes, taking into account the reduced width of the model’s Indo-Pacific basin. The  
 235 latitudinal extent of the Antipodean landmass varies between experiments, as does its at-  
 236 tachment to the southern boundary, as described in Sections 3.2 and 3.3.

## 237 2.2 Transport Streamfunction and Transport Potential

238 Typically a simple model like the one used here can have its flow described with a  
 239 transport streamfunction, which is a convenient way to diagnose flow direction and speed.  
 240 Contours of a streamfunction are parallel to the flow and changes in speed are seen as  
 241 contours coming closer together (acceleration) or further apart (deceleration). We name  
 242 the diagnostic we calculate here as the transport streamfunction since it has units of Sver-  
 243 drup.

244 The transport streamfunction described above would be defined as

$$h(\mathbf{u} + \mathbf{u}^*) = \mathbf{k} \times \nabla \psi, \quad (4)$$

245 where  $h\mathbf{u}^* = -\kappa_{GM}\nabla h$  is the bolus velocity due to the (parameterised) eddy field and  $\psi$   
 246 is the streamfunction.  $\psi$  is then obtained by integration of  $h(u + u^*)$ , the zonal thickness  
 247 transport, southwards from the northern boundary. This definition relies upon the (steady  
 248 state) zonal thickness transport being non-divergent. However, as can be seen in Equation  
 249 (2), this is not the case for our model due to the inclusion of diapycnal diffusion and deep  
 250 water formation near the southern boundary.

251 To properly account for the presence of divergent forcing in Equation (2), the thick-  
 252 ness transport must be described using a combination of a transport streamfunction and a  
 253 transport potential. This is defined by

$$h(\mathbf{u} + \mathbf{u}^*) = \mathbf{k} \times \nabla \psi + \nabla \chi, \quad (5)$$

254 where  $\chi$  is the transport potential. Like the transport streamfunction,  $\psi$ , the transport po-  
 255 tential has units of Sverdrup.

256 The portion of the flow described by the transport potential is directed across con-  
 257 tours of  $\chi$ , from low to high values. In contrast, the flow described by the transport stream-  
 258 function is along contours of  $\psi$  with high values to the right. As such, this component of  
 259 the flow is clockwise around local maxima and anticlockwise around local minima. In the  
 260 event that flow is both nondivergent and irrotational,  $\psi$  or  $\chi$  will describe the flow equally  
 261 well and only one is required; whichever is calculated second would be zero. Neverthe-  
 262 less, if both are calculated, contours of the two will cross each other at right angles.

263 To obtain the transport streamfunction and transport potential in Figure 2, we use  
 264 a Helmholtz decomposition [see, e.g., *Jayne and Marotzke, 2002; Marshall and Pillar,*  
 265 *2011*]. Beginning from Equation (5), it can be seen that

$$\nabla \cdot \{h(\mathbf{u} + \mathbf{u}^*)\} = \nabla^2 \chi. \quad (6)$$

266  $\chi$  can then be obtained using any of the many iterative solving techniques applicable to  
 267 what is essentially Poisson’s equation. Once  $\chi$  is known, its contribution to the zonal  
 268 thickness transport is calculated and removed from  $h(u + u^*)$ . The remainder is the nondi-  
 269 vergent part of the thickness transport that can be integrated meridionally to give  $\psi$ . This  
 270 follows the solution method as laid out by *Pillar [2013]*, to which the interested reader is  
 271 referred.

272 Whilst we choose to show the structure of the flow using the transport streamfunc-  
 273 tion and transport potential, it is important to remember that the total velocity is made up  
 274 of contributions from both. This means that the direction of the total flow is at a slight  
 275 angle to the contours of streamfunction, rather than strictly along them. When reporting  
 276 the transport through the model’s “Drake Passage”, we integrate the full velocity field to  
 277 avoid under-/over-reporting the volume of fluid passing through the constriction and there-  
 278 fore around the model’s “Antarctica”. In doing so, we neglect the contribution of the bolus  
 279 velocity,  $h\mathbf{u}^*$ , to the zonal transport to better reflect the transport values reported in the  
 280 literature.

### 281 2.3 Potential Vorticity

282 Potential vorticity (PV) is a useful dynamical concept that can be used to understand  
 283 complex aspects of ocean circulation in a relatively simple way. Much of this is due to  
 284 PV being largely conserved below the mixed layer, i.e. the right-hand side of it’s govern-  
 285 ing equation is (close to) zero once fluid parcels are isolated from surface forcing. Within  
 286 the mixed layer, surface wind and temperature/salinity forcing are strong, which can lead  
 287 to modification of a fluid parcel’s PV. The exact form of the PV equation depends upon  
 288 the governing equations themselves, and so must first be derived. In the case of our re-  
 289 duced gravity formulation, the form of the PV equation is well established [see, e.g., *Val-*  
 290 *lis*, 2017; *Klinger and Haine*, 2019, note that, in this context, there is little difference be-  
 291 tween the reduced gravity and shallow water equations].

292 Neglecting forcing or dissipation, on the right-hand sides of Equations (1) and (2),  
 293 the reduced gravity PV equation is given by

$$\frac{D}{Dt} \left( \frac{\xi + f}{h} \right) = 0, \quad (7)$$

294 where  $D/Dt = \partial/\partial t + (\mathbf{u} \cdot \nabla)$  is the material derivative. In the limit that  $\xi \ll f$ , i.e. that the  
 295 Rossby number is small, a condition which prevails over much of the ocean, this reduces  
 296 to

$$\frac{D}{Dt} \left( \frac{f}{h} \right) \approx 0. \quad (8)$$

297 This is a deceptively simple statement that a fluid parcel will move in such a way  
 298 as to conserve its value of  $f/h$ , as long as forcing and dissipation are weak/zero. When  
 299 bathymetry is present, which we are enclosing in our inactive bottom layer, this allows  
 300 us to understand how and where the flow will be strongly steered by the bathymetry. For  
 301 example, in the modern ocean the path of the ACC is heavily constrained by bathymetric  
 302 features, such as Kerguelan Plateau or the South-East Indian Ridge, and the steep bathymetry  
 303 in Drake Passage [see, e.g. *Mazloff et al.*, 2010]. Many of these features can be seen in  
 304 maps of the modern day ocean’s  $f/h$  contours [see, e.g., Figure 11 of *Marshall*, 2011].  
 305 In the simple channel model experiments of *Munday et al.* [2015] this can be seen in the  
 306 strong steering of the flow by the bathymetric ridge, which results in large north-south ex-  
 307 cursions of the flow. In contrast, in the flat bottomed experiments of, e.g., *Munday et al.*  
 308 [2015] or *Abernathey et al.* [2011] the mean flow is zonally symmetric, since there is no  
 309 bathymetry to steer it.

310 PV is also of great facility when considering wind-driven gyres. In the interior of  
 311 the gyre, the curl of the wind is able to modify a fluid parcel’s value of  $f/h$ . This allows  
 312 them to migrate meridionally, due to Sverdrup transport, and cross contours of  $f/h$ . In  
 313 the western boundary current region a different dynamical balance prevails, which allows  
 314 the western boundary current to close the circulation of the gyre. In the early examples of  
 315 *Stommel* [1948] and *Munk* [1950], bottom friction and viscosity are able to modify the PV  
 316 and facilitate meridional motion, i.e. the crossing of  $f/h$  contours. These terms are largest  
 317 in the western boundary region, where velocities and velocity gradients are much higher

figs/figure2-labels.pdf

333 **Figure 2.** Transport streamfunction for the reference experiments a) without deep water formation and b)  
 334 with deep water formation. Black regions are land. Positive transport streamfunction (clockwise circulation)  
 335 is solid contours, negative transport streamfunction (anticlockwise circulation) is dotted contours. Colour is  
 336 the transport potential (upgradient flow). Note that the contour interval ( $\Delta\psi$ ) for the transport streamfunction  
 337 differs in order to allow a visual comparison of the flow structure. Black arrow heads indicate the direction  
 338 of the flow along contours of transport streamfunction. Red/blue arrow heads indicate the direction of flow  
 339 perpendicular to contours of transport potential.

318 than in the Sverdrup balance-dominated interior. In the case of a sloping western bound-  
 319 ary current, a modified balance takes place and motion is unlikely to be purely meridional  
 320 [*Jackson et al.*, 2006].

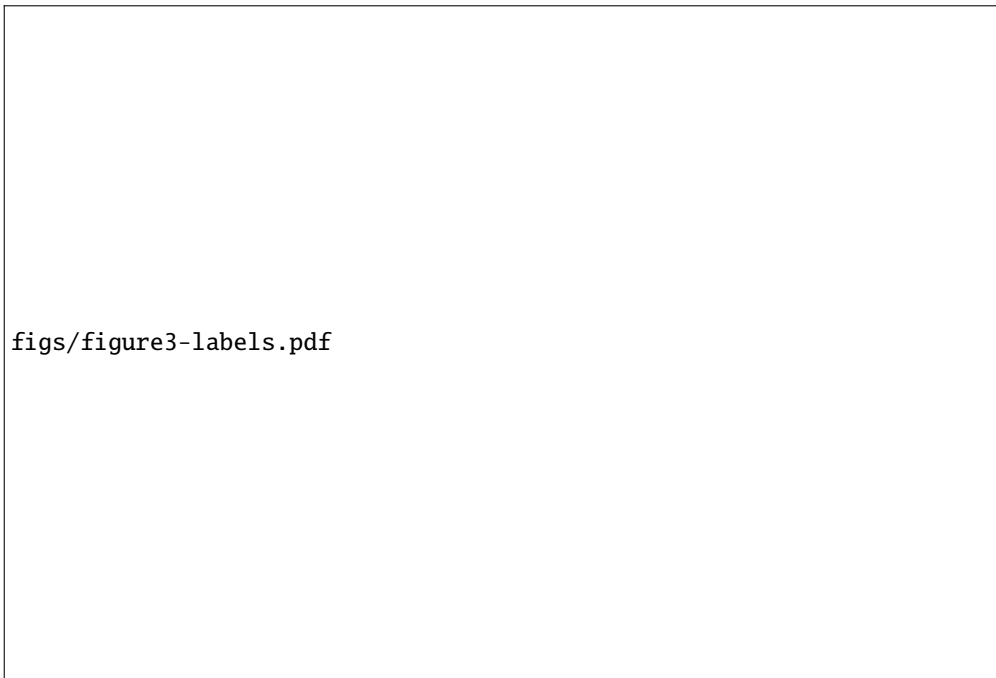
321 In the case of our simple reduced gravity model, PV remains a useful concept. The  
 322 enclosure of the bottom bathymetry in the inactive layer frees our solution from strong  
 323 bottom steering. However, the model’s contours of  $f/h$  will still intersect our idealised  
 324 continents. This implies that, in the absence of forcing and dissipation, there would be  
 325 no flow, since the boundary condition of no normal flow at the continent would project  
 326 along the  $f/h$  contour. This is an example of the profound influence of boundary condi-  
 327 tions, both in the sense that it is the no normal flow condition that would prevent flow, but  
 328 also that the addition of forcing and dissipation would free us from this constraint. In our  
 329 simple solutions, this allows us to infer things about the locations where  $f/h$  contours are  
 330 crossed and how the model dynamics allow the flow’s value of  $f/h$  to be altered to allow  
 331 this flow.

### 322 3 Model Results

#### 340 3.1 Reference Experiment

341 The reference experiment has the geometry and forcing described in Section 2.1.  
 342 The southern boundary has no Antipodean landmass, and no island in the Indo-Pacific  
 343 basin. The steady state transport streamfunction and transport potential for the reference  
 344 experiment is shown in Figure 2 both with and without southern deep water formation,  
 345 which highlights the impact of this physical process.

346 For the reference case without deep water formation, Figure 2a, a 82.3 Sv circum-  
 347 polar current flows around Antarctica. The model ACC undergoes a significant excursion  
 348 north of Drake Passage latitudes, as with the modern ACC, with its axis being roughly  
 349 aligned with the peak in the wind stress jet (at 54.5°S). The curl in the wind stress to  
 350 the north of the model’s ACC also drives a significant “supergyre” [*Speich et al.*, 2007],  
 351 with a transport of  $\sim 108$  Sv, which spans both basins north of the model’s ACC to the  
 352 southern limit of the model’s Cape Horn. The curl of the wind also leads to a gyre em-

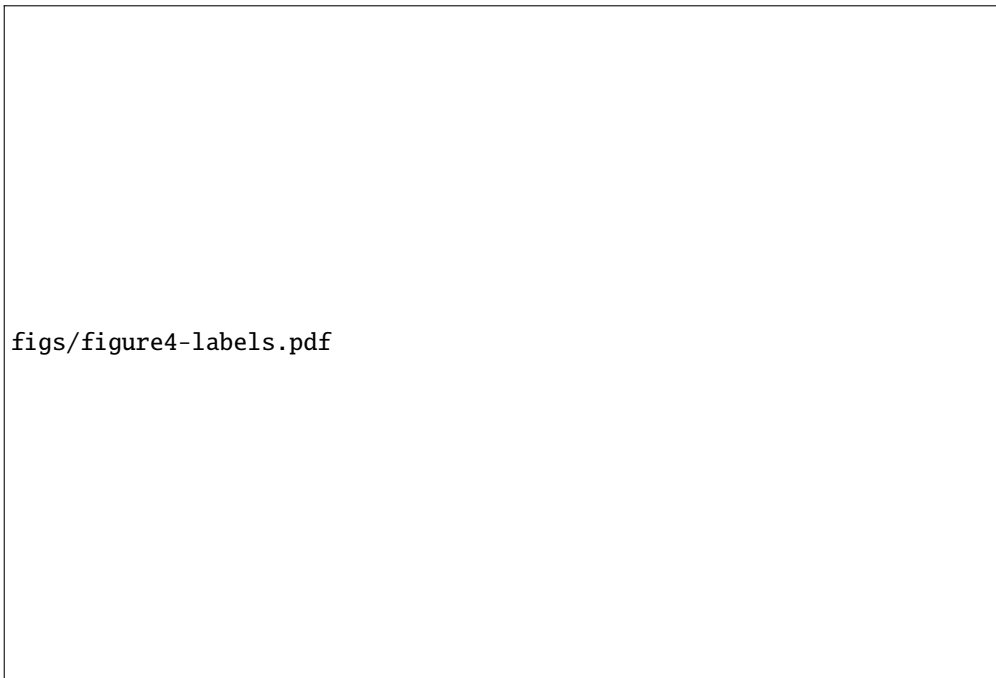


361 **Figure 3.** Transport streamfunction for a selection of closed seaway experiments without deep water for-  
 362 mation a) island extent  $8^\circ$ , b) island extent  $24^\circ$ , c) island extent  $76^\circ$  and d) island extent  $108^\circ$ . Black regions  
 363 are land. Positive transport streamfunction (clockwise circulation) is solid contours, negative transport stream-  
 364 function (anticlockwise circulation) is dotted contours. Colour is the transport potential (upgradient flow).  
 365 Note that the contour interval ( $\Delta\psi$ ) for the transport streamfunction differs in order to allow a visual compar-  
 366 ison of the flow structure. Black arrow heads indicate the direction of the flow along contours of transport  
 367 streamfunction. Red/blue arrow heads indicate the direction of flow perpendicular to contours of transport  
 368 potential.

353 bedded in the flow south of the model's ACC core. This is despite the lack of a continent  
 354 within Drake Passage latitudes. In the framework of PV, briefly laid out in Section 2.3,  
 355 the curl of the wind leads to a Sverdrup transport and drives flow across  $f/h$  contours in  
 356 the interior of the gyre. This flow is relatively slow. In the western boundary regions, the  
 357 southwards/northwards Sverdrup transport is returned northwards/southwards by a west-  
 358 ern boundary current. Given the viscous/diffusive nature of our reduced gravity model, the  
 359 meridional motion will be facilitated by viscous modification of PV, which allows the fluid  
 360 parcels to cross contours of  $f/h$ .

369 There is little flow structure, or variation in the active layer thickness, north of the  
 370 edge of the supergyre due to the lack of wind forcing at higher latitudes. Broadly speak-  
 371 ing, the reference experiment is similar to the experiments of *Allison et al.* [2010] and  
 372 *Allison et al.* [2011], at least for those in which their wind stress was placed towards the  
 373 southern boundary.

374 The addition of deep water formation near the southern boundary in Figure 2b in-  
 375 creases the circumpolar transport of the model's ACC to 270 Sv. This is due to the much  
 376 stronger meridional gradient in layer thickness caused by the deep water formation reduc-  
 377 ing it to 10m near the southern boundary. This drives a concomitantly stronger geostrophic  
 378 zonal flow eastwards. The supergyre also increases in transport from 108 Sv to 122 Sv  
 379 (counterclockwise). This is because the enhancement in the meridional gradient of layer  
 380 thickness persists across most of the model's Southern Ocean, leading to higher velocities.



384 **Figure 4.** Transport streamfunction for a selection of closed seaway experiments with deep water formation  
 385 a) island extent  $8^\circ$ , b) island extent  $24^\circ$ , c) island extent  $76^\circ$  and d) island extent  $108^\circ$ . Black regions are land.  
 386 Positive transport streamfunction (clockwise circulation) is solid contours, negative transport streamfunction  
 387 (anticlockwise circulation) is dotted contours. Colour is the transport potential (upgradient flow). Note that  
 388 the contour interval ( $\Delta\psi$ ) for the transport streamfunction differs in order to allow a visual comparison of the  
 389 flow structure. Black arrow heads indicate the direction of the flow along contours of transport streamfunc-  
 390 tion. Red/blue arrow heads indicate the direction of flow perpendicular to contours of transport potential.

381 Note that no other parameters or forcing (other than the timestep) has been changed be-  
 382 tween Figure 2a and 2b; the change in circumpolar transport can be directly attributed to  
 383 initiation of deep water formation in Figure 2b.

391 As well as increasing the circumpolar transport, the initiation of deep water forma-  
 392 tion also introduces a much stronger divergent component of the flow in Figure 2b. Di-  
 393 apycnal water mass transformation acts to increase layer thickness, largely north of the  
 394 model's Southern Ocean. However, it remains weak in both reference experiments. The  
 395 introduction of deep water formation reduces the layer thickness near the southern bound-  
 396 ary from  $\sim 250\text{m}$  to  $10\text{m}$ . This loss of volume is fed by a divergent flow that is largely  
 397 southwards, since the flow is upgradient with respect to  $\chi$ , as shown by the colour-shading  
 398 in Figure 2b. This supplies water to the deep water formation region and acts to offset the  
 399 loss of volume due to deep water formation. Broadly speaking, the divergent part of the  
 400 flow is stronger in the Pacific basin, due largely to its width. In the PV framework of Sec-  
 401 tion 2.3, the deep water formation acts as a sink/source of PV on the right-hand side of  
 402 Eq. (8). This allows the non-divergent flow to cross  $f/h$  contours and provide fluid to the  
 403 southern boundary of the model.

### 404 3.2 Closed Seaway

412 In the first set of experiments, the Antipodean landmass (Australia) remains attached  
 413 to the southern boundary (Antarctica) and its meridional extent is gradually increased. In

figs/figure5-labels.pdf

405 **Figure 5.** Transport streamfunction for the experiments with an island extent of  $140^\circ$  a) without deep wa-  
 406 ter formation and b) with deep water formation. Black regions are land. Positive transport streamfunction  
 407 (clockwise circulation) is solid contours, negative transport streamfunction (anticlockwise circulation) is dot-  
 408 ted contours. Colour is the transport potential (upgradient flow). Note that the contour interval ( $\Delta\psi$ ) for the  
 409 transport streamfunction differs in order to allow a visual comparison of the flow structure. Black arrow heads  
 410 indicate the direction of the flow along contours of transport streamfunction. Red/blue arrow heads indicate  
 411 the direction of flow perpendicular to contours of transport potential.

414 between each experiment the meridional extent of the landmass is increased by  $4^\circ$ . The  
 415 final experiment has the northern and southern boundary connected by a landmass  $140^\circ$  in  
 416 extent, such that there is no longer a zonal channel between them at any latitude. Repre-  
 417 sentative examples of transport streamfunction and transport potential for experiments with  
 418 an Antipodean landmass of  $8^\circ$ ,  $24^\circ$ ,  $76^\circ$  and  $108^\circ$  meridional extent are shown in Figures  
 419 3. None of these experiments include deep water formation.

420 Figure 3 demonstrates that as the Antipodean landmass grows, and gradually divides  
 421 the southern section of the Indo-Pacific into two, it disrupts the path of the model ACC.  
 422 Initially this provides an extra source of friction near the southern boundary (Figure 3a),  
 423 reducing the magnitude of, but still allowing, circumpolar transport. The continued growth  
 424 of the landmass goes on to disrupt the circulation of the supergyre. For landmasses of  
 425 extent greater than about  $36^\circ$ , such that the northern tip is at the same latitude as the tip  
 426 of Africa, the supergyre breaks cleanly in two with separate gyres in the Atlantic/western  
 427 Indo-Pacific and eastern Indo-Pacific. At this point the circumpolar transport has also been  
 428 reduced to near zero (see below). The Southern Ocean is now occupied by a series of  
 429 wind-driven gyres propped up by the landmasses and a new clockwise supergyre takes  
 430 up the rest of the Southern Ocean.

431 The introduction of deep water formation near the southern boundary acts to change  
 432 the character of experiments with an attached Antipodean landmass in similar ways to in  
 433 the reference experiments. As with Figure 3a, with a small Antipodean landmass an extra  
 434 source of friction is introduced and the circumpolar transport drops slightly (Figure 4a).  
 435 However, as the landmass grows in Figure 4b the axis of the ACC is pushed northwards,  
 436 rather than flow being completely blocked. Due to the steep meridional gradient in layer  
 437 thickness, a geostrophic zonal flow is still supported. Even when the Antipodean landmass  
 438 reaches the latitude of the model's Cape Agulhas, several tens of Sverdrups are able to  
 439 circulate around its Southern Ocean. When the tip of the Antipodes extends beyond the  
 440 Equator, circumpolar contours of streamfunction still exist, creating a circumpolar trans-  
 441 port of  $\sim 10$  Sv. For the flow to cross the Equator, it must change its sign of  $f/h$ . Friction  
 442 with the sidewalls provides the means to do this and promote fluid flow across the Equator.  
 443 At this point the circumpolar flow exists as a series of meridional/western boundary  
 444 layers connected by piece-wise quasi-zonal flow, much like the model of *Webb* [1993] and

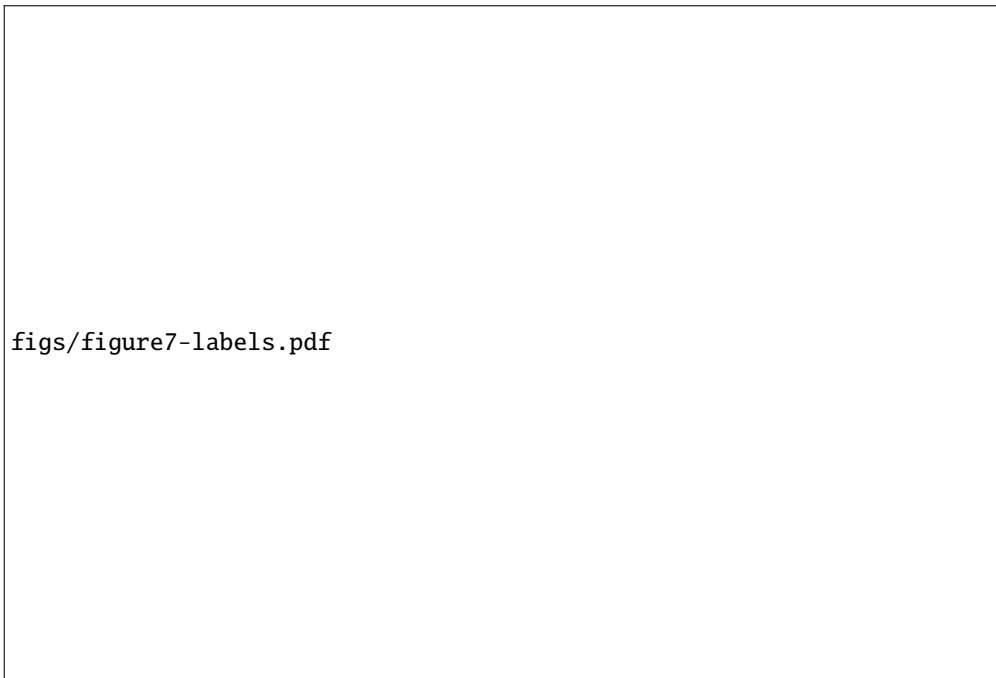
figs/figure6.pdf

446 **Figure 6.** a) Circumpolar transport as a function of the position of the Antipodean landmasses northern  
 447 edge.  $-74^\circ$  corresponds to the reference case with no island,  $65^\circ$  corresponds to the island extending to the  
 448 northern boundary. b) Circumpolar transport as a function of the position of the Antipodean landmasses  
 449 northern edge. The island land mass is  $24^\circ$  in latitude;  $-50^\circ$  corresponds to the island being attached to the  
 450 southern boundary, i.e. Island Extent of  $24^\circ$  in Figures 3b and 4b. The desaturated points in (b) are the first 6  
 451 points from (a).

445 the linear models of the ACC reviewed by *LaCasce and Isachsen* [2010].

452 For an island extent of  $140^\circ$  the divided supergyre in the northern half of the model's  
 453 Southern Ocean is very similar both with and without deep water formation, see Figure 5.  
 454 Without deep water formation there is also a supergyre in the southern half of the model's  
 455 Southern Ocean. However, when deep water formation is turned on, this supergyre is dis-  
 456 rupted by the strong meridional gradient in layer thickness. The result is very weak trans-  
 457 port streamfunction values. The divergent flow, as shown by the transport potential, is  
 458 notably stronger in Figure 5b than in Figure 4d (as shown by the strength of the colour  
 459 shading). This is an indication of stronger flow into the deep water formation region in  
 460 Figure 5b. The circumpolar transport without deep water formation is slightly westward  
 461 (negative), supported by stronger diapycnal upwelling in the Atlantic/western Pacific basin  
 462 flowing westward into the eastern Pacific. With deep water formation it remains eastward  
 463 (positive), albeit only 4.5 Sv.

464 The steady state circumpolar transport for all experiments in which the Antipodean  
 465 landmass is attached to the southern boundary is summarised in Figure 6a. In the absence  
 466 of deep water formation (red line in Figure 6a) the addition of a small Antipodes causes  
 467 a decrease in circumpolar transport. The circumpolar transport then holds roughly con-  
 468 stant until the Antipodes is  $> 12^\circ$  in extent. This can be attributed to increased friction  
 469 with the southern boundary, due to a slightly longer perimeter, and the addition of a form  
 470 stress/pressure difference across the landmass. Bottom form stress is the primary sink of  
 471 zonal momentum for the real Southern Ocean, although continental form stress can play  
 472 a role for obstructed ACC's as here [*Munday et al.*, 2015]. Once the Antipodes exceeds  
 473 this extent, the circumpolar transport decreases smoothly to almost zero as the path of  
 474 the circumpolar current becomes increasingly obstructed. The circumpolar transport can-  
 475 not recover once this has taken place and when the Antipodes extends all the way to the  
 476 northern boundary (Figure 5a) the transport is actually slightly negative (westward).

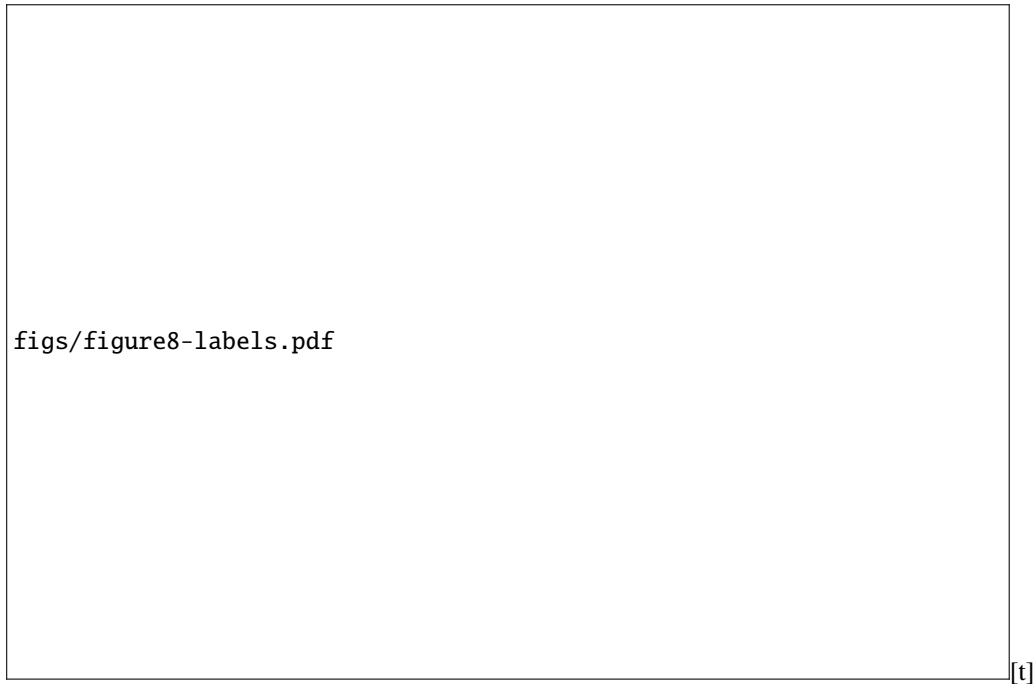


492 **Figure 7.** Transport streamfunction for a selection of open seaway experiments without deep water forma-  
 493 tion a) seaway extent  $24^\circ$ , b) seaway extent  $48^\circ$ , c) seaway extent  $72^\circ$  and d) seaway extent  $96^\circ$ . Black regions  
 494 are land. Positive transport streamfunction (clockwise circulation) is solid contours, negative transport stream-  
 495 function (anticlockwise circulation) is dotted contours. Colour is the transport potential (upgradient flow).  
 496 Note that the contour interval ( $\Delta\psi$ ) for the transport streamfunction differs in order to allow a visual compar-  
 497 ison of the flow structure. Black arrow heads indicate the direction of the flow along contours of transport  
 498 streamfunction. Red/blue arrow heads indicate the direction of flow perpendicular to contours of transport  
 499 potential.

477 The addition of deep water formation increases the circumpolar transport of the refer-  
 478 ence case from 82.3 Sv to 270.0 Sv (blue line in Figure 6a). The decrease with the ad-  
 479 dition of a small Antipodes is very rapid, with the transport reaching 132.8 Sv for an An-  
 480 tipodes  $12^\circ$  in extent. The subsequent decrease in circumpolar transport as the Antipodes  
 481 continues to grow persists across all the experiments. Even when the Antipodes extends  
 482 across the Equator the circumpolar transport is 11.6 Sv. This is because the deep wa-  
 483 ter formation continues to enforce a strong meridional gradient in layer thickness, which  
 484 contributes to the geostrophic zonal flow. The formation of meridional boundary layers  
 485 is then able to funnel fluid across the Equator by viscous modification of the fluid's PV,  
 486 which allows flow to cross  $f/h$  contours. Even when the Antipodes extends all the way to  
 487 the northern boundary the transport remains slightly eastward (positive), in contrast to the  
 488 case without deep water formation. This is due to preferential deep water formation tak-  
 489 ing place in the Indo-Pacific due to its width. Water must then flow from the Atlantic, via  
 490 Drake Passage, to compensate the lost layer thickness due to the restoring. This creates an  
 491 eastward (positive) Drake Passage transport.

### 500 3.3 Open Seaway

509 In the second set of experiments, an Antipodean landmass of meridional extent  $24^\circ$   
 510 is separated from the southern boundary and gradually moved northwards (representing  
 511 the Tasmanian Seaway). In between each experiment, the landmass is moved  $4^\circ$  farther



501 **Figure 8.** Transport streamfunction for a selection of open seaway experiments with deep water formation  
502 a) seaway extent  $24^\circ$ , b) seaway extent  $48^\circ$ , c) seaway extent  $72^\circ$  and d) seaway extent  $96^\circ$ . Black regions are  
503 land. Positive transport streamfunction (clockwise circulation) is solid contours, negative transport stream-  
504 function (anticlockwise circulation) is dotted contours. Colour is the transport potential (upgradient flow).  
505 Note that the contour interval ( $\Delta\psi$ ) for the transport streamfunction differs in order to allow a visual compar-  
506 ison of the flow structure. Black arrow heads indicate the direction of the flow along contours of transport  
507 streamfunction. Red/blue arrow heads indicate the direction of flow perpendicular to contours of transport  
508 potential.

512 north. Experiments with and without deep water formation are performed and are shown  
513 in Figures 7 and 8, respectively.

514 In the absence of deep water formation the change in basin topology due to an An-  
515 tipodean landmass of  $24^\circ$  meridional extent breaking away from the southern boundary  
516 makes little difference to the circumpolar transport or the qualitative features of the cir-  
517 culation (cf. Figures 7a and 3b). The Southern Ocean is still dominated by a pair of su-  
518 pergyres, although it is only the southernmost that is split completely in two by the An-  
519 tipodes. When the Antipodes is  $8^\circ$  away from the southern boundary in Figure 7b, the cir-  
520 cumpolar flow shifts to the southern side of the Antipodes and decreases slightly in terms  
521 of circumpolar transport at the model Drake Passage. As the Antipodes continues to move  
522 northwards the circumpolar transport is able to increase due to the removal of a large ob-  
523 stacle to the flow. Once the Antipodes is clear of the latitudes of significant circumpolar  
524 flow, any further movement northwards does little to the transport. As demonstrated in  
525 Figures 7c and 7d, there is also little change in the structure and path of the streamlines.

526 The divergent part of the flow, as shown by the colour shading for  $\chi$ , remains weak  
527 in Figure 7, just as in Figure 3, and is concentrated around the exit from Drake Passage.  
528 Here the total flow is strong and this sharp turn leads to large horizontal divergence and  
529 thus large gradients in  $\chi$ . Despite this, the flow remains largely non-divergent, as shown  
530 by the contours of  $\psi$  and largely constant values of  $\chi$  elsewhere in the domain.

531 The initiation of deep water formation in Figure 8 leads to a strengthening of cir-  
532 cumpolar transport for all seaway extents. As the island migrates away from the southern  
533 boundary, the restoration of the layer thickness to  $h^*$  quickly leads to the majority of its  
534 transport occurring on its southern side. With only  $4^\circ$  between the southern boundary and  
535 the southern edge of the landmass (Figure 8a), approximately  $2/3$  of the total transport of  
536 the current passes to the south of the landmass. Once the island's southern boundary is  
537 north of about  $50^\circ\text{S}$ , the presence of the island has little further impact upon the model  
538 ACC, as shown in Figure 8c for the case of the seaway being the same width as the is-  
539 land. However, the supergyre continues to be disrupted.

540 The steady state circumpolar transport for all experiments in which a  $24^\circ$  Antipodean  
541 landmass is detached from the southern boundary and moved northwards is summarised in  
542 Figure 6b. We repeat the first six points from Figure 6a, as the Antipodes is growing to  
543  $24^\circ$  in extent, to highlight how the subsequent detachment of the Antipodes changes the  
544 downwards trend.

545 When the Antipodes is first detached ( $4^\circ$  seaway), the circumpolar transport does not  
546 increase straight away without deep water formation. In fact, it drops to roughly the same  
547 level as growing the Antipodes such that its northern edge is at the same latitude ( $28^\circ$  is-  
548 land). However, subsequent widening of the seaway leads to rapid growth of the circum-  
549 polar transport. Both with and without deep water formation the circumpolar transport is  
550 on par with that of the reference simulation when the northern edge of the detached An-  
551 tipodes is level with the southern edge of “Africa”. The circumpolar transport actually  
552 overshoots slightly when the Antipodes is moved a further  $4^\circ$  northwards before decreas-  
553 ing to match the reference case once more.

#### 554 **4 Summary and Discussion**

555 The timeframe in which Drake Passage opened between Cape Horn and the Antarc-  
556 tic continent is poorly constrained [e.g. *Barker and Thomas, 2004*]. In contrast, the open-  
557 ing of the Tasman Gateway is relatively well-dated to between 35.5Ma and 30Ma [*Barker*  
558 *et al., 2007*]. In the past, the literature has sometimes assumed that a belt of open circum-  
559 polar latitudes is a prerequisite for the formation of a circumpolar current. However, re-  
560 cent theoretical advances regarding the path and transport of the ACC have shown that it  
561 can migrate a considerable distance north of any open circumpolar latitude band in order

562 to follow the wind forcing [Allison *et al.*, 2010]. This suggests that in deep paleo-time, it  
 563 may have been possible for a considerable circumpolar current to have formed prior to the  
 564 opening of the Tasman Gateway if Drake Passage was already open. The model of *Sauer-*  
 565 *milch et al.* [2021] does not produce circumpolar flow when the Tasman Gateway is closed  
 566 and the domain extended to the Equator. However, with Eocene temperature and salinity  
 567 forcing, the density gradient across the Southern Ocean remains lower than in the modern  
 568 world. This leads them to suggest that the initiation, and/or strengthening, of deep water  
 569 formation due to buoyancy loss may allow for both a stronger circumpolar transport and  
 570 circumpolar flow with the Tasman Gateway closed.

571 Using a simple reduced gravity model with idealised geometry and forcing, we have  
 572 demonstrated that deep water formation is crucial in setting the circumpolar transport. For  
 573 large Antipodean landmasses attached to the southern boundary, deep water formation is  
 574 able to elevate the circumpolar transport to several tens of Sverdrups. Importantly, even  
 575 with a closed seaway, circumpolar transport is possible due to flow along the north-side  
 576 of the Antipodean landmass. Deep water formation is even able to allow for some, albeit  
 577 very small, circumpolar transport when the Antipodes extends beyond the Equator with a  
 578 series of viscous boundary layers enabling the cross-Equatorial flow.

579 Considering the plate tectonic framework from the Cretaceous to the early Ceno-  
 580 zoic, this scenario may have been possible. According to *van de Lagemaat et al.* [2021],  
 581 the Drake Passage may have been open during the Cretaceous and closed again later,  
 582 whilst the Tasman Gateway remained closed until some time in the Eocene (50Ma, ac-  
 583 cording to e.g. [Bijl *et al.*, 2013]). During this time period between the Cretaceous and the  
 584 Eocene, Australia and Antarctica experienced late rifting and ultra-slow seafloor spread-  
 585 ing from west to east with the Tasman Gateway being the last section to separate [e.g.  
 586 *Sauermilch et al.*, 2019]. During this tectonic process, the northern section of the Aus-  
 587 tralian plate subsided below the Pacific Plate and, consequently, narrowed the Indonesian  
 588 Seaway with time. However, previous studies suggest that the Indonesian Seaway still re-  
 589 mained a significant width and depth until at least 25Ma [e.g. *Gaina and Müller*, 2007].  
 590 Based on various global paleogeography reconstructions, it can be expected that the lat-  
 591 itudes of the northern part of Australia and the southern tip of Africa were not too far  
 592 off from each other (with Australia not moving north of the equator). According to our  
 593 model results, this would allow a certain ACC transport via the Indonesian Seaway and  
 594 the already open Drake Passage since the Cretaceous, even without deep water formation  
 595 (see Figure 3). Assuming that deep water formation developed around or even prior to the  
 596 Eocene [see, e.g. *Hague et al.*, 2012; *Thomas*, 2004; *Thomas et al.*, 2014; *Via and Thomas*,  
 597 2006; *McKinley et al.*, 2019], it may be possible that a stronger ACC developed, poten-  
 598 tially even before the Tasman Gateway opened, with Australia moving farther north and  
 599 the Indonesian Seaway narrowing (see Figure 4). It should be noted that our model indi-  
 600 cates that only a narrow Tasman Gateway is necessary for circumpolar flow to switch to  
 601 this southern pathway. This suggests that it would be early in the history of the gateway's  
 602 tectonic opening and deepening that flow would have begun.

603 In the case of a detached Antipodean landmass progressively moved to the north, the  
 604 transport increases until it is fully recovered to that of the reference experiment. With the  
 605 smallest separation between landmass and southern boundary considered,  $4^\circ$  or  $\sim 400\text{km}$ ,  
 606 most of the circumpolar transport is achieved by a strong eastwards flow between the  
 607 southern boundary and the landmass. Whilst the modern ACC has a volume transport in  
 608 excess of 130 Sv, a transport of several 10's of Sverdrups would still place such a flow  
 609 amongst the strongest currents in the modern world. For example, as it flows through  
 610 Florida Strait, the transport of the Florida Current is  $32.2 \pm 3.3$  Sv [*Meinen et al.*, 2010],  
 611 which rises to  $\sim 70 - 75$  Sv after separation from Cape Hatteras as the Gulf Stream [*Hei-*  
 612 *derich and Todd*, 2020]. Other western boundary currents show similar transports, such as  
 613 the  $< 11$  Sv of the Brazil Current between  $12^\circ\text{S}$  and  $25^\circ\text{S}$  [*Imawaki et al.*, 2013], or the  
 614 East Australian Current's  $22.1 \pm 7.5$  Sv at  $27^\circ\text{S}$  [*Sloyan et al.*, 2016]. In this context, the

615 Drake Passage transports of  $\sim 42 - 44$  Sv achieved in the Rupelian geometries of *Hill et al.*  
 616 [2013] are quite impressive. It seems likely that it would not be necessary for Australia  
 617 to have reached its modern latitude prior to the inception of a circumpolar current with a  
 618 volume transport placing it amongst the most powerful currents on Earth, as long as deep  
 619 water formation has also begun/strengthened in the Southern Ocean.

620 The changes in the path and transport of the model ACC observed in both sets of  
 621 experiments have important implications for several aspects of the real ACC. For exam-  
 622 ple, an ACC that migrates to the degree seen here could have a considerably different  
 623 set of transport properties for heat, salt and other climatically important tracers such as  
 624 carbon or nutrients. Quantifying the impact of a weak circumpolar current in a warmer  
 625 climate requires more sophisticated models than a reduced gravity model. Furthermore,  
 626 mesoscale eddies are of great importance to the circulation of the Southern Ocean, both  
 627 in terms of the dynamical balance that sets the volume transport of the ACC [*Munk and*  
 628 *Palmén*, 1951; *Johnson and Bryden*, 1989] and the meridional overturning circulation that  
 629 accompanies it [*Marshall and Radko*, 2003]. A proper assessment of the changing prop-  
 630 erties of such circumpolar currents therefore requires the use of an eddy-resolving ocean  
 631 model at an increase in computing cost of several orders of magnitude. Even in the ab-  
 632 sence of complex forcing and an increase in the number of vertical levels, reducing the  
 633 grid spacing of the reduced gravity model used here from  $1^\circ$  to  $1/10^\circ$  would increase the  
 634 computational cost by a factor of roughly 1000.

635 Restoring our reduced gravity model to a shallow thickness near the southern bound-  
 636 ary is a very simplified version of deep water formation. Recent global models, at reso-  
 637 lutions requiring the parameterisation of mesoscale eddies, differ in their opinion of the  
 638 overturning regime, and thus bottom water formation site, of the Eocene ocean [e.g. *Hu-*  
 639 *ber and Sloan*, 2001; *Huber and Nof*, 2006; *Sijp et al.*, 2011]. This may suggest a role for  
 640 multiple equilibria due to salt advection [*Stommel*, 1961; *Marotzke and Willebrand*, 1991;  
 641 *Hawkins et al.*, 2011] or sea-ice albedo [*Budyko*, 1969; *Sellers*, 1969; *Ferreira et al.*, 2011]  
 642 feedbacks in producing warm equable climates. This can allow for a sudden transition be-  
 643 tween warm and cold climates with very different circulations [*Rose et al.*, 2013; *Rose*,  
 644 2015]. If multiple equilibria were possible under Eocene geometry and forcing, then it  
 645 may explain the differences between contemporaneous simulations with one existing in a  
 646 “warm” state and the other in a “cold” state. Both salt advection and sea-ice albedo are  
 647 known to be modified by changes in ocean geometry [*von der Heydt and Dijkstra*, 2008;  
 648 *Ferreira et al.*, 2011], with sea-ice albedo equilibria being linked to glacial/interglacial cy-  
 649 cles [*Ferreira et al.*, 2018]. How multiple equilibria might also be modified by the presence  
 650 of a vigorous mesoscale eddy field is yet to be determined.

## 651 5 Open Research

652 The model code used for the numerical experiments is available from Zenodo [*Mun-*  
 653 *day*, 2022]. Model output is available from the Open Science Framework at <https://osf.io/pqymu/>  
 654 [*Munday et al.*, 2022].

## 655 Acknowledgments

656 DRM was supported by the Natural Environment Research Council [ORCHESTRA, grant  
 657 number NE/N018095/1]. This work used JASMIN, the UK’s collaborative data analysis  
 658 environment [see <https://jasmin.ac.uk>, *Lawrence et al.*, 2013]. Isabel Sauer-  
 659 milch acknowledges funding through the ERC starting grant n802835 OceaNice. The initial experiments  
 660 were conducted when DRM was a PDRA at the University of Oxford, supported by the  
 661 Natural Environment Research Council. This research was partially supported by the Aus-  
 662 tralian Government through the Australian Research Council’s Discovery Projects funding  
 663 scheme (project DP180102280).

## References

- 664
- 665 Abernathey, R., J. Marshall, and D. Ferreira (2011), The dependence of Southern Ocean  
666 meridional overturning on wind stress., *J. Phys. Oceanogr.*, *41*, 2261–2278.
- 667 Adcroft, A., and D. Marshall (1998), How slippery are piecewise-constant coastlines in  
668 numerical ocean models?, *Tellus*, *50*, 95–108.
- 669 Allison, L. C. (2009), Spin-up and adjustment of the Antarctic Circumpolar Current and  
670 global pycnocline., Ph.D. thesis, Univ. Reading.
- 671 Allison, L. C., H. L. Johnson, D. P. Marshall, and D. R. Munday (2010), Where do  
672 winds drive the Antarctic Circumpolar Current?, *Geophys. Res. Lett.*, *37*, L12,605,  
673 doi:10.1029/2010GL043,355.
- 674 Allison, L. C., H. L. Johnson, and D. P. Marshall (2011), Spin-up and adjustment of  
675 the Antarctic Circumpolar Current and global pycnocline., *J. Mar. Res.*, *69*, 167–189,  
676 doi:10.1357/002224011798765,330.
- 677 Baatsen, M. L. J., A. S. von der Heydt, M. Kliphuis, J. Viebahn, and H. A. Dijkstra  
678 (2018), Multiple states in the late Eocene ocean circulation., *Global Planet. Change*,  
679 *163*, 18–28, doi: 10.1016/j.gloplacha.2018.02.009.
- 680 Barker, P. F., and E. Thomas (2004), Origin, signature and palaeoclimatic influence of the  
681 Antarctic Circumpolar Current., *Earth-Sci. Rev.*, *66*, 143–162.
- 682 Barker, P. F., B. Diekmann, and C. Escutia (2007), Onset of Cenozoic Antarctic glacia-  
683 tion., *Deep-Sea Res.*, *54*, 2293–2307.
- 684 Bijl, P. K., J. A. P. Bendle, S. M. Bohaty, J. Pross, S. Schouten, L. Tauxe, C. E. Stickley,  
685 R. M. McKay, U. Röhl, M. Olney, A. Sluijs, C. Escutia, H. Brinkhuis, and Expedition  
686 318 Scientists (2013), Eocene cooling linked to early flow across the Tasmanian Gate-  
687 way., *Proc. Natl. Acad. Sci.*, *110*, 9645–9650m, doi:10.1073/pnas.1220872,110.
- 688 Borrelli, C., B. S. Cramer, and M. E. Katz (2014), Bipolar Atlantic deepwater circulation  
689 in the middle-late eocene: Effects of Southern Ocean gateway openings., *Paleoceanogr.*  
690 *Paleoclimatol.*, *29*, 308–327, doi:10.1002/2012PA002,444.
- 691 Budyko, M. I. (1969), The effect of solar radiation variations on the climate of the Earth.,  
692 *Tellus*, *21*, 611–619.
- 693 Donohue, K. A., K. L. Tracey, D. R. Watts, M. P. Chidichimo, and T. K. Chereskin  
694 (2016), Mean Antarctic Circumpolar Current transport measured in Drake Passage.,  
695 *Geophys. Res. Lett.*, *43*, 11 760–11 767, doi:10.1002/2016GL070,319.
- 696 Durran, D. R. (1991), The third-order Adams-Bashforth method: An attractive alternative  
697 to leapfrog time differencing., *Mon. Wea. Rev.*, *119*, 702–720.
- 698 Ferreira, D., J. Marshall, and B. Rose (2011), Climate determinism revisited: Multiple  
699 equilibria in a complex climate model., *J. Clim.*, *24*, 992–1012.
- 700 Ferreira, D., J. Marshall, T. Ito, and D. McGee (2018), Linking glacial-interglacial  
701 states to multiple equilibria of climate., *Geophys. Res. Lett.*, *45*, 9160–9170,  
702 doi:10.1029/2018GL077,019.
- 703 Gaina, C., and D. Müller (2007), Cenozoic tectonic and depth/age evolution of the  
704 Indonesian gateway and associated back-arc basins., *Earth-Sci. Rev.*, *83*, 177–203,  
705 doi:10.1016/j.earscirev.2007.04.004.
- 706 Gent, P. R., and J. C. McWilliams (1990), Isopycnal mixing in ocean circulation models.,  
707 *J. Phys. Oceanogr.*, *20*, 150–155.
- 708 Gnanadesikan, A. (1999), A simple predictive model for the structure of the oceanic pyc-  
709 noclone., *Science*, *283*, 2077–2079.
- 710 Goldner, A., N. Herold, and M. Huber (2014), Antarctic glaciation caused ocean  
711 circulation changes at the Eocene-Oligocene transition., *Nature*, *511*, 574–577,  
712 doi:10.1038/nature13,597.
- 713 Hague, A. M., D. J. Thomas, M. Huber, R. Korty, S. C. Woodard, and L. B. Jones (2012),  
714 Convection of North Pacific deep water during the early Cenozoic., *Geology*, *40*, 527–  
715 530, doi:10.1130/G32,886.1.
- 716 Hawkins, E., R. S. Smith, L. C. Allison, J. M. Gregory, T. J. Woollings, H. Pohlmann,

- 717 and B. de Cuevas (2011), Bistability of the Atlantic overturning in a global climate  
718 model and links to ocean freshwater transport., *Geophys. Res. Lett.*, *38*, L10,605,  
719 doi:10.1029/2011GL047,208.
- 720 Heiderich, J., and R. E. Todd (2020), Along-stream evolution of Gulf Stream volume  
721 transport., *J. Phys. Oceanogr.*, *50*, 2251–2270, doi:10.1175/JPO–D–19–0303.1.
- 722 Hill, D. J., A. M. Haywood, P. J. Valdes, J. E. Francis, D. J. Lunt, B. S. Wade, and V. C.  
723 Bowman (2013), Paleogeographic controls on the onset of the Antarctic circumpolar  
724 current., *Geophys. Res. Lett.*, *40*, 5199–5204, doi:10.1002/grl.50,941.
- 725 Huber, M., and D. Nof (2006), The ocean circulation in the southern hemisphere and its  
726 climatic impacts in the Eocene., *Palaeogeogr., Palaeoclimatol., Palaeoecol.*, *231*, 9–28.
- 727 Huber, M., and L. C. Sloan (2001), Heat transport, deep waters, and thermal gradients:  
728 Coupled simulation of an Eocene Greenhouse Climate., *Geophys. Res. Lett.*, *28*, 3481–  
729 3484.
- 730 Huck, C. E., T. van de Fliedrt, S. M. Bohaty, and S. J. Hammond (2017), Antarctic  
731 climate, Southern Ocean circulation patterns, and deep water formation during the  
732 Eocene., *Paleoceanogr. Paleoclimatol.*, *32*, 674–691, 10.1002/2014PA003,135.
- 733 Hutchinson, D. K., A. M. de Boer, H. K. Coxall, R. Caballero, J. Nilsson, and M. Baatsen  
734 (2018), Climate sensitivity and meridional overturning circulation in the late Eocene  
735 using GFDL CM2.1., *Clim. Past*, *14*, 789–810, doi:10.5194/cp–14–789–2018.
- 736 Imawaki, S., A. S. Bower, L. Beal, and B. Qiu (2013), *Western boundary currents.*, *Inter-*  
737 *national Geophysics series*, vol. 103, chap. 13, pp. 305–330, Academic Press, London,  
738 UK.
- 739 Jackson, L., C. W. Hughes, and R. G. Williams (2006), Topographic control of basin and  
740 channel flows: The role of bottom pressure torques and friction., *J. Phys. Oceanogr.*, *36*,  
741 1786–1805.
- 742 Jayne, S. R., and J. Marotzke (2002), The oceanic eddy heat transport., *J. Phys.*  
743 *Oceanogr.*, *32*, 3328–3345.
- 744 Johnson, G. C., and H. L. Bryden (1989), On the size of the Antarctic Circumpolar Cur-  
745 rent., *Deep-Sea Res.*, *36*, 39–53.
- 746 Katz, M. E., B. S. Cramer, J. R. Toggweiler, G. Esmay, C. Liu, K. G. Miller, Y. Rosen-  
747 thal, B. S. Wade, and J. D. Wright (2011), Impact of Antarctic Circumpolar Cur-  
748 rent development on late Paleogene ocean structure., *Science*, *332*, 1076–1079,  
749 doi:10.1126/science.1202,122.
- 750 Kennett, J. P. (1977), Cenozoic evolution of Antarctic glaciation, the circum-Antarctic  
751 ocean, and their impact on global paleoceanography., *J. Geophys. Res.*, *82*, 3843–3860.
- 752 Klinger, B., and T. Haine (2019), *Ocean Circulation in Three Dimensions*, Cambridge Uni-  
753 versity Press, 466 pp, doi:10.1017/9781139015721.
- 754 LaCasce, J. H., and P. E. Isachsen (2010), The linear models of the ACC., *Prog.*  
755 *Oceanogr.*, *84*, 139–157.
- 756 Lawrence, B. N., V. L. Bennet, J. Churchill, M. Jukes, P. Kershaw, S. Pascoe, S. Pe-  
757 ppler, M. Pritchard, and A. Stephens (2013), Storing and manipulating environmental  
758 big data with JASMIN., in *2013 IEEE International Conference on Big Data*, pp. 68–75,  
759 doi:10.1109/BigData.2013.6691,556.
- 760 Livermore, R., A. Nankivell, G. Eagles, and P. Morris (2005), Paleogene opening of Drake  
761 Passage., *Earth Planet. Sci. Lett.*, *236*, 459–470.
- 762 Marotzke, J., and J. Willebrand (1991), Multiple equilibria of the global thermohaline cir-  
763 culation., *J. Phys. Oceanogr.*, *21*, 1372–1385.
- 764 Marshall, D. (1995), Topographic steering of the Antarctic Circumpolar Current., *J. Phys.*  
765 *Oceanogr.*, *25*, 1636–1650.
- 766 Marshall, D. P. (2011), Rossby wormholes., *J. Mar. Res.*, *69*, 309–330,  
767 doi:10.1357/002224011798765,213.
- 768 Marshall, D. P., and H. R. Pillar (2011), Momentum balance of the wind-driven and  
769 meridional overturning circulation., *J. Phys. Oceanogr.*, *41*, 960–978.
- 770 Marshall, D. P., D. R. Munday, L. C. Allison, R. J. Hay, and H. L. Johnson (2016), Gill’s

- 771 model of the Antarctic Circumpolar Current, revisited: The role of latitudinal variations  
772 in wind stress., *Ocean Model.*, *97*, 37–51, doi:10.1016/j.ocemod.2015.11.010.
- 773 Marshall, J., and T. Radko (2003), Residual-mean solutions for the Antarctic Circumpolar  
774 Current and its associated overturning circulation., *J. Phys. Oceanogr.*, *33*, 2341–2354.
- 775 Mazloff, M. R., P. Heimbach, and C. Wunsch (2010), An eddy-permitting Southern Ocean  
776 State Estimate., *J. Phys. Oceanogr.*, *40*, 880–899, doi:10.1175/2009JPO4236.1.
- 777 McKinley, C. C., D. J. Thomas, L. J. LeVay, and Z. Rolewicz (2019), Nd isotopic struc-  
778 ture of the Pacific Ocean 40–10 Ma and evidence for the reorganization of deep North  
779 Pacific Ocean circulation between 36 and 35 Ma., *Earth Planet. Sci. Lett.*, *521*, 139–149,  
780 doi:10.1016/j.epsl.2019.06.009.
- 781 Meinen, C. S., M. O. Baringer, and R. F. Garcia (2010), Florida Current transport vari-  
782 ability: An analysis of annual and longer-period signals., *Deep-Sea Res.*, *57*, 835–846,  
783 doi:10.1016/j.dsr.2010.04.001.
- 784 Meredith, M. P., P. L. Woodworth, T. K. Chereskin, D. P. Marshall, L. C. Allison, G. R.  
785 Bigg, K. Donohue, K. J. Heywood, C. W. Hughes, A. Hibbert, A. M. Hogg, H. L.  
786 Johnson, B. A. King, H. Leach, Y. Lenn, M. A. Morales-Maqueda, D. R. Munday,  
787 A. C. Naveira-Garabato, C. Provost, and J. Sprintall (2011), Sustained monitoring of the  
788 Southern Ocean at Drake Passage: past achievements and future priorities, *Rev. Geo-  
789 phys.*, *49*, RG4005, doi:10.1029/2010RG000348.
- 790 Munday, D. (2022), davemunday/reducedgravity: v1.0.1, doi:10.5281/zenodo.7078679.
- 791 Munday, D. R., H. L. Johnson, and D. P. Marshall (2015), The role of ocean gateways in  
792 the dynamics and sensitivity to wind stress of the early Antarctic Circumpolar Current.,  
793 *Paleoceanography*, *30*, 284–302, doi:10.1002/2014PA002675.
- 794 Munday, D. R., I. Sauermilch, J. Whittaker, and A. Klocker (2022), Opening of Tasman  
795 Seaway and the Antarctic Circumpolar Current, p. doi:10.17605/OSF.IO/PQYMU.
- 796 Munk, W. H. (1950), On the wind-driven ocean circulation., *J. Meteorol.*, *7*, 79–93.
- 797 Munk, W. H., and E. Palmén (1951), Note on the dynamics of the Antarctic Circumpolar  
798 Current., *Tellus*, *3*, 53–55.
- 799 Nof, D. (2000), Does the wind control the import and export of the South Atlantic?, *J.*  
800 *Phys. Oceanogr.*, *30*, 2650–2666.
- 801 Nof, D. (2002), Is there a meridional overturning cell in the Pacific and Indian oceans?, *J.*  
802 *Phys. Oceanogr.*, *32*, 1947–1959.
- 803 Nof, D. (2003), The Southern Ocean’s grip on the northward meridional flow., *Prog.*  
804 *Oceanogr.*, *56*, 223–247.
- 805 Pillar, H. R. (2013), Sensitivity of the Atlantic Meridional Overturning Circulation to Sur-  
806 face Forcing, Ph.D. thesis, University of Oxford, Oxford, UK.
- 807 Rose, B. E. J. (2015), Stable “Waterbelt” climates controlled by tropical ocean heat trans-  
808 port: A nonlinear coupled climate mechanism of relevance to Snowball Earth., *J. Geo-  
809 phys. Res.*, *120*, 1404–1423, doi:10.1002/2014DJ022659.
- 810 Rose, B. E. J., D. Ferreira, and J. Marshall (2013), The role of oceans and sea ice  
811 in abrupt transitions between multiple climate states., *J. Clim.*, *26*, 2862–2879,  
812 doi:10.1175/JCLI-D-12-00175.1.
- 813 Royer, J. Y., and N. Rollet (1997), Plate-tectonic setting of the Tasmanian region., *Aust. J.*  
814 *Earth Sci.*, *44*, 543–560, doi:10.1080/08120099708728336.
- 815 Sauermilch, I., J. M. Whittaker, P. K. Bijl, J. M. Totterdell, and W. Jokat (2019), Tec-  
816 tonic, oceanographic, and climatic controls on the Cretaceous-Cenozoic sedimen-  
817 tary record of the Australian-Antarctic basin., *J. Geophys. Res.*, *124*, 7699–7724,  
818 doi:10.1029/2018JB016683.
- 819 Sauermilch, I., J. M. Whittaker, A. Klocker, D. R. Munday, K. Hochmuth, J. H. LaCasce,  
820 and P. K. Bijl (2021), Gateway-driven weakening of ocean gyres leads to Southern  
821 Ocean cooling, *Nat. Commun.*, *12*, 6465, doi:10.1038/s41467-021-26658-1.
- 822 Scher, H. D., and E. E. Martin (2006), Timing and climatic consequences of the opening  
823 of Drake Passage., *Science*, *312*, 428–430, doi:10.1126/science.1120044.
- 824 Scher, H. D., J. M. Whittaker, S. E. Williams, J. C. Latimer, W. E. Kordesch, and M. L.

- 825 Delaney (2015), Onset of Antarctic Circumpolar Current 30 million years ago as tasma-  
 826 nian gateway aligned with westerlies., *Nature*, 523, 580–583, doi:10.1038/nature14,598.
- 827 Sellers, W. D. (1969), A global climatic model based on the energy balance of the earth-  
 828 atmosphere system., *J. Appl. Met.*, 8, 392–400.
- 829 Sijp, W. P., M. H. England, and M. Huber (2011), Effect of the deepening of  
 830 the Tasman Gateway on the global ocean., *Paleoceanography*, 26, PA4207,  
 831 doi:10.1029/2011PA002,143.
- 832 Sijp, W. P., A. S. von der Heydt, H. A. Dijkstra, S. Flögel, P. M. J. Douglas, and P. K.  
 833 Bijl (2014), The role of ocean gateways on cooling climate on long time scales., *Global*  
 834 *Planet. Change*, 119, 1–22, doi: 10.1016/j.gloplacha.2014.04.004.
- 835 Sloyan, B. M., K. R. Ridgway, and R. Cowley (2016), The East Australian Current and  
 836 property transport at 27°S from 2012 to 2013., *J. Phys. Oceanogr.*, 46, 993–100,  
 837 doi:10.1175/JPO–D–15–0052.1.
- 838 Speich, S., B. Blanke, and W. Cai (2007), Atlantic meridional overturning circu-  
 839 lation and the Southern Ocean supergyre., *Geophys. Res. Lett.*, 34, L23,614,  
 840 doi:10.1029/2007GL031,583.
- 841 Stickley, C. E., H. Brinkhuis, S. A. Schellenberg, A. Sluijs, U. Röhl, M. Fuller,  
 842 M. Grauert, M. Huber, J. Warnaar, and G. L. Williams (2004), Timing and na-  
 843 ture of the deepening of the Tasmanian Gateway., *Paleoceanography*, 19, PA4027,  
 844 doi:10.1029/2004PA001,022.
- 845 Stommel, H. (1948), The westward intensification of wind-driven ocean currents., *Trans.*  
 846 *Amer. Geophys. Union*, 29, 202–206.
- 847 Stommel, H. (1961), Thermohaline circulation with two stable regimes of flow, *Tellus*, 13,  
 848 224–230.
- 849 Thomas, D. J. (2004), Evidence for deep-water production in the North Pacific ocean dur-  
 850 ing the early Cenozoic warm interval., *Nature*, 430, 65–68, doi:10.1038/nature02,639.
- 851 Thomas, D. J., R. Korty, M. Huber, J. A. Schubert, and B. Haines (2014), Nd isotopic  
 852 structure of the Pacific Ocean 70–30 Ma and numerical evidence for vigorous ocean cir-  
 853 culation and ocean heattransport in a greenhouse world., *Paleoceanography*, 29, 454–  
 854 469, doi:10.1002/2013PA002,535.
- 855 Vallis, G. (2017), *Atmospheric and Oceanic Fluid Dynamics*, Cambridge University Press,  
 856 946 pp, doi:10.1017/9781107588417.
- 857 van de Lagemaat, S. H. A., M. L. A. Swart, B. Vaes, M. E. Kusters, L. M. Boschman,  
 858 A. Burton-Johnson, P. K. Bijl, W. Spakman, and D. J. J. van Hinsbergen (2021), Sub-  
 859 duction initiation in the Scotia Sea region and opening of the Drake Passage: When and  
 860 why?, *Earth-Sci. Rev.*, 215, 103,551, doi:10.1016/j.earscirev.2021.103,551.
- 861 Via, R. K., and D. J. Thomas (2006), Evolution of Atlantic thermohaline circulation: Early  
 862 Oligocene onset of deep-water production in the North Atlantic, *Geology*, 34, 441–444,  
 863 doi:10.1130/G22,545.1.
- 864 von der Heydt, A., and H. A. Dijkstra (2008), The effect of gateways on ocean  
 865 circulation patterns in the Cenozoic., *Global Planet. Change*, 62, 132–146,  
 866 doi:10.1016/j.gloplacha.2007.11.006.
- 867 Webb, D. J. (1993), A simple model of the effect of the Kerguelen Plateau on the strength  
 868 of the Antarctic Circumpolar Current., *Geophys. Astrophys. Fluid Dynam.*, 70, 57–84,  
 869 doi:10.1080/03091929308203,587.
- 870 Wei, W., and S. W. Wise (1992), Eocene-Oligocene calcareous nannofossil magneto-  
 871 biochronology of the Southern Ocean, *Newsl. Stratigr.*, 26, 119–132.
- 872 Westerhold, T., N. Marwan, A. J. Drury, D. Liebrand, C. Agnini, E. Anagnostou, J. S. K.  
 873 Barnett, S. M. Bohaty, D. De Vleeschouwer, F. Florindo, T. Frederichs, D. A. Hodell,  
 874 A. E. Holbourn, D. Kroon, V. Laurentino, K. Littler, L. J. Lourens, M. Lyle, H. Pälike,  
 875 U. Röhl, J. Tian, R. H. Wilkens, P. A. Wilson, and J. C. Zachos (2020), An astronomi-  
 876 cally dated record of Earth’s climate and its predictability over the last 66 million years,  
 877 *Science*, 369, 1383–1387, doi:10.1126/science.aba6853.